Fermi National Accelerator Laboratory

FERMILAB–Pub–88/54–T

June 1988

QCD radiative corrections to the photoproduction of heavy quarks

R. K. Ellis

Fermi National Accelerator Laboratory

P. O. Box 500, Batavia, Illinois 60510

P. Nason

Institute of Theoretical Physics,

ETH - Hönggerberg,

Zurich, Switzerland

June 5, 1988

Abstract

We present the results of a full calculation of the QCD $\mathcal{O}(\alpha_S^2\alpha_{em})$ radiative corrections to the heavy quark photoproduction cross section. Explicit formulae are given for the total cross-section for the photoproduction of a heavy quark pair due to photon-parton fusion. Using our results we present estimates of the differential and total cross-section for the photoproduction of charm. Within the large theoretical uncertainties the calculated charm photoproduction cross section is in reasonable agreement with present data. We show that the cross section for the photoproduction of bottom is reliably calculable.

Operated by Universities Research Association Inc. under contract with the United States Department of Energy

1. Introduction

In this paper we consider the production of heavy quarks by a beam of real photons. Our results should be useful in the description of photoproduction experiments at fixed target energies. In addition they can be used to describe the production of heavy quarks at HERA, because in the absence of electron tagging, HERA can be considered as a facility providing a wide band beam of quasi-real photons. We work in the context of the QCD parton model and give results for the first QCD radiative correction to the lowest order photon-gluon fusion formula. These results are analogous to the $\mathcal{O}(\alpha_S^3)$ results obtained in ref. [1] by Nason, Dawson and Ellis for the hadroproduction of heavy quarks.

The standard perturbative QCD formula for the inclusive production of a heavy quark Q of momentum p and energy E,

$$\gamma(P_1) + H(P_2) \to Q(p) + X \tag{1.1}$$

determines the invariant cross-section as follows,

$$\frac{E\, d^3\sigma}{d^3p} = \sum_j \int dx \left[\frac{E\, d^3\hat{\sigma}_{\gamma j}(P_1, xP_2, p, m, \mu)}{d^3p}\right] F_j^H(x,\mu)$$
$$+ \sum_{i,j} \int dx_1 dx_2 \left[\frac{E\, d^3\hat{\sigma}_{ij}(x_1P_1, x_2P_2, p, m, \mu)}{d^3p}\right] F_i^\gamma(x_1,\mu)\, F_j^H(x_2,\mu) \tag{1.2}$$

The functions F_j^H and F_i^γ are the number densities of light partons (gluons, light quarks and antiquarks) in a hadron and photon respectively, evaluated at a scale μ. The symbol $\hat{\sigma}$ denotes the short distance cross-section from which the mass singularities have been factored. After factorisation, the sensitivity to momentum scales below the heavy quark mass has been removed and $\hat{\sigma}$ is calculable as a perturbation series in $\alpha_S(\mu^2)$. The scale μ is *a priori* only determined to be of the order of the mass m of the produced heavy quark. Eq. (1.2) is the full result in QCD up to corrections which are suppressed by powers of the heavy quark mass[2]. We will refer to the first term in eq. (1.2) as the pointlike contribution of the photon, while the remaining term will be referred to as the hadronic contribution. The separation of the two terms is controlled by the scale μ. Singularities due to the splitting of the photon into massless partons with a transverse momentum less than $\mathcal{O}(\mu)$ are

reabsorbed into the hadronic component. The splitting of the photon into partons with a transverse momentum larger than $\mathcal{O}(\mu)$ is included in the pointlike contribution. In almost all the phenomenological applications of our formulae it will turn out that the hadronic component is numerically small. We will therefore mention it only where necessary. The radiative corrections associated with the hadronic component are exactly the same as in hadroproduction of heavy quarks. They are discussed in ref. [1].

The first term in the perturbation series which contributes to the pointlike component is $\mathcal{O}(\alpha_S \alpha_{\rm em})$. $\alpha_{\rm em}$ is the electromagnetic fine structure constant. At this order the only process which contributes to heavy quark production is photon-gluon fusion.

$$\gamma + g \rightarrow Q + \overline{Q}. \tag{1.3}$$

The diagrams contributing to the lowest order cross-section are shown in Fig. 1. The invariant matrix elements squared and the cross-sections for these processes have been available in the literature for some time[3,4]. Lowest order predictions for the photon-hadron cross-sections are obtained by inserting these parton cross-sections (together with the appropriate parton cross-sections for the hadronic component) into eq. (1.2).

The phenomenological consequences of the lowest order formulae can be summarised as follows. The average transverse momentum of the heavy quark or antiquark is of the order of its mass and the p_T distribution falls rapidly to zero as p_T becomes larger than the heavy quark mass. The rapidity difference between the produced quark and antiquark is predicted to be of order one.

The matrix elements squared for the photoproduction of a heavy quark pair plus a light parton have also been calculated[5]. By themselves, they have physical significance only when the jet associated with the light parton has a large transverse momentum. When the produced light parton has small transverse momentum the matrix elements contain collinear and soft divergences, which cancel only when the virtual corrections to the diagrams of Fig. 1 are included, and the factorisation procedure is carried out.

In this paper we present the results of a full calculation of the inclusive photoproduction cross-section for heavy quark production to order $\alpha_S^2 \alpha_{\rm em}$. We have calculated the short distance cross-sections $\hat{\sigma}$ for the inclusive production of a heavy quark of transverse momentum p_T and rapidity y. This requires the calculation of the cross-

sections for the following parton inclusive processes,

$$\gamma + g \to Q + X,\ \gamma + q \to Q + X,\ \gamma + \overline{q} \to Q + X \tag{1.4}$$

The inclusive cross-sections for the production of an anti-quark $\overline{Q}$ differ from those for the production of a quark Q at a given y and p_T. This effect[6], which first arises in $\mathcal{O}(\alpha_S^2\alpha_{\rm em})$, is expected to be small in most kinematic regions. Using eq. (1.2) we calculate the distributions in rapidity and transverse momentum of produced heavy quarks correct through $\mathcal{O}(\alpha_S^2\alpha_{\rm em})$. The exclusive parton sub-processes which contribute to the inclusive cross-sections are,

$$\begin{aligned}
\gamma + g &\to Q + \overline{Q}, && \alpha_S\alpha_{\rm em},\ \alpha_S^2\alpha_{\rm em} \\
\gamma + g &\to Q + \overline{Q} + g, && \alpha_S^2\alpha_{\rm em} \\
\gamma + q &\to Q + \overline{Q} + q, && \alpha_S^2\alpha_{\rm em} \\
\gamma + \overline{q} &\to Q + \overline{Q} + \overline{q}, && \alpha_S^2\alpha_{\rm em}.
\end{aligned} \tag{1.5}$$

Note the necessity of including both real and virtual gluon emission diagrams in order to calculate the $\mathcal{O}(\alpha_S^2\alpha_{\rm em})$ photon gluon inclusive cross-section.

From our results for the one heavy quark inclusive cross-section we have derived the total cross-section for the inclusive production of a heavy quark pair calculated to order $\mathcal{O}(\alpha_S^2\alpha_{\rm em})$. Integrating eq. (1.2) over the momentum p we obtain,

$$\begin{aligned}
\sigma(S) = &\sum_j \int dx\ \hat{\sigma}_{\gamma j}(xS, m^2, \mu^2)\ F_j^H(x,\mu) \\
&+ \sum_{i,j} \int dx_1 dx_2\ \hat{\sigma}_{ij}(x_1x_2S, m^2, \mu^2)\ F_i^\gamma(x_1,\mu) F_j^H(x_2,\mu),
\end{aligned} \tag{1.6}$$

where S is the square of the centre of mass energy of the colliding photon-hadron system. The total short distance cross-section $\hat{\sigma}$ for the inclusive production of a heavy quark due to the collision of a photon with a parton of type j can be written as,

$$\hat{\sigma}_{\gamma j}(s, m^2, \mu^2) = \frac{\alpha_{\rm em}\alpha_S(\mu^2)}{m^2} f_{\gamma j}\Big(\rho, \frac{\mu^2}{m^2}\Big), \tag{1.7}$$

with $\rho = 4m^2/s$, and s the square of the partonic centre of mass energy. μ is the renormalisation and factorisation scale. Eq. 1.7 is analogous to the definition of the

short distance cross-section for the hadroproduction of heavy quarks,

$$\hat{\sigma}_{ij}(s, m^2, \mu^2) = \frac{\alpha_S^2(\mu^2)}{m^2} f_{ij}\Big(\rho, \frac{\mu^2}{m^2}\Big). \tag{1.8}$$

Full details of the first two terms in the perturbative expansion of the function f_{ij} are given in ref. [1]. In this paper we present a complete description of the functions $f_{\gamma j}$ including the first non-leading correction. These may be used by the reader to calculate the total rate for heavy quark photoproduction at any energy and heavy quark mass.

The remainder of this paper is organized as follows: in section II we give all the relevant formulas for the functions $f_{\gamma j}$. In section III we present the application of our formulae to the photoproduction of heavy quarks in fixed target experiments.

2. The total parton cross-section

In this section we present our results which describe the total parton cross-section for the photo-production of a heavy quark pair. The presentation parallels the one in ref. [1]. Knowledge of the functions $f_{\gamma j}$ defined in eq. (1.7) gives a complete description of the short distance cross-section for the production of a heavy quark of mass m. The index j specifies the type of the incoming parton. The dimensionless functions $f_{\gamma j}$ have the following perturbative expansion,

$$f_{\gamma j}\Big(\rho, \frac{\mu^2}{m^2}\Big) = f_{\gamma j}^{(0)}(\rho) + g^2(\mu^2)\Big[f_{\gamma j}^{(1)}(\rho) + \overline{f}_{\gamma j}^{(1)}(\rho)\ln(\frac{\mu^2}{m^2})\Big] + \mathcal{O}(g^4) \tag{2.1}$$

In order to calculate the $f_{\gamma j}$ in perturbation theory we must perform both renormalisation and factorisation of mass singularities. The subtractions required for renormalisation and factorisation are both done at mass scale μ. The dependence on μ is shown explicitly in eq. (2.1). Further μ dependence is also present in the parton distribution functions, (*cf.*eq. (1.6)) and in the coupling constant, (*cf.*eq. (1.7)). The energy dependence of the cross-section is given in terms of the ratio ρ,

$$\rho = \frac{4m^2}{s}, \quad \beta = \sqrt{1-\rho}. \tag{2.2}$$

The running of the coupling constant α_S is determined by the renormalisation group,

$$\frac{d\alpha_S(\mu^2)}{d\ln\mu^2} = -b_0\alpha_S^2 - b_1\alpha_S^3 + \mathcal{O}(\alpha_S^4), \quad \alpha_S = \frac{g^2}{4\pi}, \quad b_0 = \frac{(33-2n_{lf})}{12\pi}, \quad b_1 = \frac{(153-19n_{lf})}{24\pi^2} \tag{2.3}$$

where n_{lf} is the number of light flavours. Our results should be used in conjunction with the running coupling as defined in eq. (2.3) and together with light parton densities evolved using the two loop $\overline{MS}$ evolution equations[7]. The renormalisation scheme we have used is the same as in ref. [1] where further details can be found.

We now present a complete description of the functions $f^{(0)}, \overline{f}^{(1)}$ and $f^{(1)}$ for all the contributing parton subprocesses. The functions $f_{\gamma j}^{(0)}$ defined in eqs. (1.7,2.1) depend on the charge of the quark which interacts with the photon. In order to make these dependences explicit we define the quantities,

$$\begin{aligned} f_{\gamma g}(\rho, \frac{\mu^2}{m^2}) &= e_Q^2 c_{\gamma g}(\rho, \frac{\mu^2}{m^2}) \\ f_{\gamma q}(\rho, \frac{\mu^2}{m^2}) &= e_Q^2 c_{\gamma q}(\rho, \frac{\mu^2}{m^2}) + e_q^2 d_{\gamma q}(\rho, \frac{\mu^2}{m^2}) \end{aligned} \tag{2.4}$$

The charges of the heavy and light quarks are denoted by e_Q and e_q respectively. The interference term proportional to $e_Q e_q$ makes no contribution to the total cross-section. The perturbative expansions of c and d are defined by a formula with exactly the same structure as eq. (2.1). For the lowest order terms we find,

$$c_{\gamma g}^{(0)}(\rho) = \frac{\pi\beta\rho}{4}\left[\frac{1}{\beta}(3-\beta^4)\ln\left(\frac{1+\beta}{1-\beta}\right) - 4 + 2\beta^2\right] \tag{2.5}$$

$$c_{\gamma q}^{(0)}(\rho) = d_{\gamma q}^{(0)}(\rho) = c_{\gamma \bar{q}}^{(0)}(\rho) = d_{\gamma \bar{q}}^{(0)}(\rho) = 0. \tag{2.6}$$

In order to deal with the case in which the incoming photon fragments into a light quark-antiquark pair we also need the quantity $f_{q\bar{q}}^{(0)}$,

$$f_{q\bar{q}}^{(0)}(\rho) = \frac{\pi\beta\rho}{27}\left[2+\rho\right]. \tag{2.7}$$

$f_{q\bar{q}}^{(0)}$ is the lowest order term in the expansion of $f_{q\bar{q}}$ which was defined in eq. (1.8).

We now turn to the higher order corrections in eq. (2.1) which are separated into two terms. The $\overline{f}^{(1)}(\rho)$ terms are the coefficients of $\ln(\mu^2/m^2)$ and are determined by

renormalisation group arguments from the lowest order cross-sections,

$$\overline{f}^{(1)}_{\gamma j}(\rho) = \frac{1}{8\pi^2}\left[2\pi\, b_0\, f^{(0)}_{\gamma j}(\rho) - \sum_k \int_\rho^1 dz_1 f^{(0)}_{kj}(\frac{\rho}{z_1}) P_{k\gamma}(z_1) - \sum_k \int_\rho^1 dz_2 f^{(0)}_{\gamma k}(\frac{\rho}{z_2}) P_{kj}(z_2)\right]. \tag{2.8}$$

Using the explicit forms[8] for the lowest order Altarelli-Parisi kernels P_{ij},

$$\begin{aligned}
P_{g\gamma}(x) &= 0 \\
P_{q\gamma}(x) &= 3e_q^2\left[(x^2+(1-x)^2\right] \\
P_{gq}(x) &= \frac{4}{3}\left[\frac{1+(1-x)^2}{x}\right] \\
P_{gg}(x) &= 6\left[\frac{x}{(1-x)_+} + \frac{1-x}{x} + x(1-x)\right] + 2\pi b_0 \delta(1-x)
\end{aligned} \tag{2.9}$$

and eqs. (2.5,2.6,2.7), we find the following analytic results for the functions $\overline{c}^{(1)}_{\gamma j}(\rho)$ and $\overline{d}^{(1)}_{\gamma j}(\rho)$, functions,

$$\begin{aligned}
\overline{c}^{(1)}_{\gamma g} = \frac{1}{8\pi^2}\Bigg[\frac{\pi}{4}\Bigg\{ &-\frac{\beta}{6}(112-250\rho+285\rho^2) - \frac{\rho}{4}(72-72\rho+47\rho^2)\ln\left(\frac{1+\beta}{1-\beta}\right) \\
&+3\rho(\rho^2+2\rho-4)h_1(\beta) - 6\rho(\rho^2-2\rho-2)h_2(\beta)\Bigg\} + 6c^{(0)}_{\gamma g}(\rho)\ln\left(\frac{\rho}{4\beta^2}\right)\Bigg]
\end{aligned} \tag{2.10}$$

$$\begin{aligned}
\overline{c}^{(1)}_{\gamma q} &= \frac{1}{8\pi^2}\frac{\pi}{3}\left[\rho(\rho-2)h_1(\beta) - \frac{4}{9}\beta(14-29\rho+3\rho^2) - \frac{2}{3}\rho(3+\rho^2)\ln\left(\frac{1+\beta}{1-\beta}\right)\right] \\
\overline{d}^{(1)}_{\gamma q} &= \frac{1}{8\pi^2}\frac{\pi\beta\rho}{27}\left[(\frac{9}{2}\rho^2-6)\frac{1}{\beta}\ln\left(\frac{1+\beta}{1-\beta}\right) + 16 - 13\rho\right]
\end{aligned} \tag{2.11}$$

where the auxiliary functions h_1 and h_2 are given by,

$$\begin{aligned}
h_1(\beta) &= \ln^2\left(\frac{1+\beta}{2}\right) - \ln^2\left(\frac{1-\beta}{2}\right) + 2\,\mathrm{Li}_2\left(\frac{1+\beta}{2}\right) - 2\,\mathrm{Li}_2\left(\frac{1-\beta}{2}\right) \\
h_2(\beta) &= \mathrm{Li}_2\left(\frac{2\beta}{1+\beta}\right) - \mathrm{Li}_2\left(\frac{-2\beta}{1-\beta}\right) \\
\mathrm{Li}_2(x) &= -\int_0^x \frac{dz}{z}\ln(1-z).
\end{aligned} \tag{2.12}$$

The quantities $f^{(1)}_{\gamma j}$ in eq. (2.1) can only be obtained by performing a complete $\mathcal{O}(\alpha_{\mathrm{em}}\alpha_S^2)$ calculation. We do not have exact analytical results for the quantities

	$c_{\gamma g}^{(1)}$	$c_{\gamma q}^{(1)}$	$d_{\gamma q}^{(1)}$
a_0	0.549300	0.0693678	0.0353008
a_1	-0.0489397	-2.97841	-0.0538177
a_2	-1.38705	0.0906588	-0.0161513
a_3	-3.20322	-0.295498	0.0329156
a_4	-1.83915	-1.50046	-0.0394947
a_5	1.13247	0.501042	0.000441385
a_6	-0.669051	-1.30918	-0.00375370
a_7	-2.30483	-0.349512	0.00897664

Table 1: Coefficients in the fits for $f_{\gamma j}^{(1)}$.

$f^{(1)}$. Instead we provide a physically motivated fit to the numerically integrated result. Near the endpoints we impose the correct asymptotic behaviour. Elsewhere our fit agrees with the numerically integrated result to better than 1%. The forms of our fits are,

$$c_{\gamma g}^{(1)} = \frac{41\beta}{36\pi} + \frac{\rho}{16\pi}\left[6\beta\ln^2(8\beta^2) - 30\beta\ln(8\beta^2) - \frac{\pi^2}{6}\right]$$
$$+\beta\rho\Big[a_0 + \beta^2\Big(a_1\ln^2(8\beta^2) + a_2\ln(8\beta^2)\Big) + a_3\beta^2 + \rho\Big(a_4\ln\rho + a_5\ln^2\rho\Big)$$
$$+a_6\ln^2\rho + a_7\ln\rho\Big] \tag{2.13}$$

$$c_{\gamma q}^{(1)} = \frac{41\beta^3}{81\pi} + \rho\Big[\beta^3\Big(a_0\ln\beta + a_1\Big) + \beta^5\Big(a_2\ln\beta + a_3\Big) + \beta\rho\Big(a_4\ln\rho + a_5\ln^2\rho\Big)$$
$$+\beta\Big(a_6\ln\rho + a_7\ln^2\rho\Big)\Big] \tag{2.14}$$

$$d_{\gamma q}^{(1)} = \rho\Big[\beta^3\Big(a_0\ln\beta + a_1\Big) + \beta^5\Big(a_2\ln\beta + a_3\Big) + \beta\rho\Big(a_4\ln\rho + a_5\ln^2\rho\Big)$$
$$+\beta\Big(a_6\ln\rho + a_7\ln^2\rho\Big)\Big] \tag{2.15}$$

The coefficients in the fit are given in Table 1.

The functions $c^{(0)}, c^{(1)}$ and $\overline{c}^{(1)}$ are shown plotted in fig. 2 for the case of photon-gluon scattering. In figs. 3 and 4 we plot $c^{(1)}, \overline{c}^{(1)}, d^{(1)}$ and $\overline{d}^{(1)}$ for the case photon-

quark scattering. At high energy we find that,

$$c_{\gamma g}^{(1)} \to 3\frac{41}{108\pi} + \mathcal{O}(\rho \ln^2 \rho)$$
$$c_{\gamma q}^{(1)} \to \frac{4}{3}\frac{41}{108\pi} + \mathcal{O}(\rho \ln^2 \rho). \qquad (2.16)$$

Thus the cross-section goes to a constant as $s \to \infty$, in complete analogy with the hadroproduction case[1]. This behaviour is due to vector exchange in the t channel. The diagrams which dominate in the high energy limit are shown in fig. 5. The asymptotic values of $c_{\gamma g}^{(1)}$ and $c_{\gamma q}^{(1)}$ are proportional to the colour charge of the line which provides the exchanged gluon, since the upper blob in fig. 5 is the same for both diagrams and, in the high energy limit, the lower vertex can be approximated by an eikonal form. The ratio of the gluon and quark charges, explains the relative factor of 9/4, shown in eq. (2.16) and evident in figs. 2 and 3. At high energy the functions $\bar{c}_{\gamma g}^{(1)}$ and $\bar{c}_{\gamma q}^{(1)}$ also tend to a constant. Again the ratio is 9/4 as can be seen from eqs.(2.10,2.11).

Near threshold,($\beta \to 0$), we have,

$$c_{\gamma g}^{(1)} \to \mathcal{N}_{\gamma g}\left[-\frac{\pi^2}{6} + \beta\left(6\ln^2(8\beta^2) - 30\ln(8\beta^2)\right) + \mathcal{O}(\beta)\right]$$
$$c_{\gamma q}^{(1)} \to \mathcal{O}(\beta)$$
$$d_{\gamma q}^{(1)} \to \mathcal{O}(\beta). \qquad (2.17)$$

The normalisation, $\mathcal{N}_{\gamma g}$ of the expression in eq. (2.17) is determined as follows,

$$\mathcal{N}_{\gamma g} = \frac{1}{8\pi^2}\frac{c_{\gamma g}^{(0)}(\rho)}{\beta}\bigg|_{\beta=0} = \frac{1}{16\pi}. \qquad (2.18)$$

Notice that in this order in perturbation theory the cross-section is finite at threshold. This is due to the $1/\beta$ coulomb singularity. A similar behaviour was found in the hadroproduction case.

The sharp rise of the terms $c^{(1)}$ near the threshold is mostly due to the $\ln^2(\beta)$ terms shown in eq. (2.17). Terms of this sort are in part responsible for the large radiative corrections to the Drell-Yan process[9]. In fact, these terms are quite general in nature[1] and in this case are associated with the incoming gluon line. Since in

hadroproduction we have two incoming gluons, whereas in photoproduction there is only one, we expect that the coefficient of the $ln^2(\beta)$ terms in hadroproduction will be twice as large as the corresponding coefficient in photoproduction. This is in fact the case[1]. It is also interesting to note that in the high energy limit ($\rho \to 0$), the ratios of the correction terms in hadroproduction and photoproduction are approximately equal.

$$\begin{aligned} \frac{f_{gg}^{(1)}(\rho)}{\overline{f}_{gg}^{(1)}(\rho)} &\approx -2.7 \\ \frac{c_{\gamma g}^{(1)}(\rho)}{\overline{c}_{\gamma g}^{(1)}(\rho)} &\approx -2.0 \end{aligned} \tag{2.19}$$

Indeed, the corrections to the γg subprocess are very similar to the corrections to the gg subprocess, once allowance has been made for the differing number of gluons in the initial state. This suggests that the large corrections to the cross-section can be associated with the incoming gluon line.

We obtain the hadronic cross-section from our partonic cross-section according to the formula eq. (1.6). One of the most important contributions to the cross-section comes from the photon-gluon fusion mechanism. In order to get an idea of the importance of the various terms it is useful to plot the product of the the photon-gluon cross-section $\sigma_{\gamma g}(xs, m^2, \mu^2)$ and gluon density per unit of rapidity $xG(x)$. Since this exercise is only intended to be illustrative, we have chosen a gluon distribution given by,

$$xG(x) = 3(1-x)^5 \tag{2.20}$$

The resulting product is the cross-section per unit of rapidity of the incoming gluon. In fig. 6 we have plotted this quantity for charm production at a photon energy of 200 GeV corresponding to 19.4 GeV in the centre of mass frame. In fig. 7 we illlustrate the situation for charm production at HERA by choosing a total centre of mass energy 314 GeV, corresponding to the most energetic photon possible. We take the charm mass to be 1.5 GeV. It is clear from the figures that as the energy gets higher the radiative corrections become more important than the lowest order term to an extent controlled by the available rapidity gap. This effect, unimportant at fixed target energies, is already visible at HERA energies.

3. Phenomenological applications

We now turn our attention to the photoproduction of charm at fixed target energies. According to eqs. (1.2) and (1.6) the physical cross-section depends on both the hadronic and point-like components of the photon. To the order to which we are working a complete calculation requires the inclusion of the radiative corrections[1] to the parton-parton mechanism of heavy quark production. We have verified that the contribution from the hadronic component of the photon is small at fixed target energies. Using the parameterisation of the photon structure functions given in Ref. 10, we find that the hadronic component for charm production is always less than 5% for $50 < E_\gamma < 400$ GeV. We will therefore neglect it when discussing the production of charm at fixed target energies.

Before discussing our results for the photoproduction of charm we shall discuss the uncertainties in the QCD prediction. The first uncertainty is whether the photon-gluon fusion model, together with the QCD corrections contained in this paper, can describe the photoproduction of charm at all. The expansion parameter is the charm quark mass, which may not be big enough compared to the QCD scale Λ to give reliable results. The phenomenological analysis given below should therefore be viewed as an attempt to describe the data rather than a definitive test of the theory. A related uncertainty is the value of the mass of the heavy quark. The dependence of the cross-section on the mass of the charmed quark is particularly important at fixed target energies. The basic question which the data on charm photoproduction must address is quite simple. Is it possible to find a value of the charmed quark mass using which the QCD parton model can describe the data?

The uncertainties in the parameters other than the heavy quark mass, (μ, Λ and the form of the gluon distribution) lead to smaller variations so we discuss them first. If we choose the scale $\mu < 2m_c$ we enter into a region in which the gluon distributions are not measured. In fact, if we try to extrapolate the gluon densities from present data using the Altarelli-Parisi evolution equations we find large instabilities. The extrapolated result depends strongly upon the initial condition. In order to avoid this problem, we will use mainly the value $\mu \approx 2m_c$. The uncertainties associated with the choice of a lower value for μ will be simply assumed to be of the order of a factor of two.

The other source of uncertainty is the lack of a precise knowledge of the value of Λ, and the form of the gluon distribution. There is a strong correlation in these parameters. Our treatment of this uncertainty follows the analysis given in ref. [12]. The running coupling is defined in terms of $\Lambda_{n_{lf}}$ (in the $\overline{MS}$ scheme) as,

$$\alpha_S(\mu^2, n_{lf}) = \frac{1}{b_{0,n_{lf}} \ln(\mu^2/\Lambda^2_{n_{lf}})}\left[1 - \frac{b_{1,n_{lf}}}{b^2_{0,n_{lf}}} \frac{\ln\ln(\mu^2/\Lambda^2_{n_{lf}})}{\ln(\mu^2/\Lambda^2_{n_{lf}})}\right] \tag{3.1}$$

where $b_{0,n_{lf}}$ and $b_{1,n_{lf}}$ depend on the number of active light flavours as shown in eq. (2.3). Observe that the value of α_S and the value of $\Lambda_{\overline{MS}}$ both depend on the number of active flavours. In the $\overline{MS}$ scheme the relationship between $\Lambda_{n_{lf}}$ and $\Lambda_{n_{lf}+1}$ is determined by the equation,

$$\alpha_S(m^2_{n_{lf}+1}, n_{lf}+1) = \alpha_S(m^2_{n_{lf}+1}, n_{lf}) \tag{3.2}$$

where $m_{n_{lf}+1}$ is the mass of the quark which is becoming active. We assume the following uncertainty in Λ_4,

$$\Lambda_4 = 260 \pm 100 \text{ MeV}. \tag{3.3}$$

The corresponding ranges for Λ_5 and Λ_3 are,

$$\begin{aligned} \Lambda_5 &= \quad 170 \pm 80 \text{ MeV} \\ \Lambda_3 &= \quad 310 \pm 110 \text{ MeV} \end{aligned} \tag{3.4}$$

and the three corresponding forms of the gluon distribution function as given in ref. [11]. Our estimates of the errors due to variations of μ (estimated using the factor of two explained above) and the variation of Λ (and the gluon distribution) are added in quadrature, to give the outer lines in figs. 8,9 and 10. The middle curve corresponds to the choice $\Lambda_4 = 260$ GeV, $\mu^2 = 10$ GeV^2; it should not be construed as a preferred value and is included only for definiteness. The estimate of the theoretical error is somewhat arbitrary, but those presented in the figures give the right order of magnitude. Because of the mass dependence of the result, we have chosen to quote our cross sections for different values of the charmed quark mass of 1.2, 1.5 and 1.8 GeV. Figs. 8, 9 and 10 also show experimental values for the total cross-section. The majority of the experimental points are taken from the compilation

given in ref. [13], where references to the original papers can be found. Also included are new points[14] from Fermilab experiment E691. From these figures it is clear that even with the large theoretical uncertainties one can distinguish between different values of the quark mass. The value of 1.5 GeV is quite adequate, while the smaller value seems to be ruled out by the data. Note that the mass value preferred by QCD sum rules[15] is $m = 1.46 \pm 0.5$ GeV.

We now turn to the differential distributions for the production of charmed quarks. Fig. 11 shows the x_F distribution, including lowest order and next-to-leading order terms. Higher order terms do not substantially modify the shape of the x_F distribution. From fig. 11 we can derive the x_F distribution for D-mesons by including the Peterson phenomenological fragmentation function.

$$D(z) = \frac{1}{z}\left(1 - \frac{1}{z} - \frac{\epsilon}{(1-z)}\right)^{-2} \tag{3.5}$$

Figs. 11 and 12 show that the shape of the x_F distribution is substantially unchanged by the inclusion of the first non-leading correction. In fig. 13 we show the p_T^2 distribution for three values of the heavy quark mass. The shape of the p_T spectrum is also little changed by the inclusion of radiative corrections. In figs. 11, 12 and 13 the choice $\mu^2 = 10$ GeV^2 has been made.

From a theoretical standpoint the photoproduction of bottom is much more reliably calculable. In fig. 14 the dependence on the subtraction scale μ is displayed. In lowest order the predicted cross section varies substantially with μ. After inclusion of the radiative corrections the total variation of the cross-section is less than a factor of two for choices of μ in the range $m/2 < \mu < 2m$. In fig. 15 we show the total cross section for the production of bottom as a function of the photon beam energy. The band of values shown represents the theoretical uncertainty due to the variation of the scale μ between $m_b/2$ and $2m_b$, the variation of Λ (and the gluon distribution function) in the range given by eq. (3.3), and the variation of the bottom quark mass between 4.5 and 5 GeV.

We now turn to the production of bottom quarks at the electron-proton facility HERA. We have calculated the cross-section for the production of bottom quarks at a total centre of mass energy $\sqrt{S} = 314$ GeV; we get a cross section of 6 ± 1.1 nb. The errors have been estimated in the same way as for the calculation of fixed target bottom photoproduction. The photon spectrum at HERA was calculated using the

m_c (GeV)	σ (μb)	+	−
1.2	1.24	.53	.35
1.5	.68	.26	.18
1.8	.41	.14	.10

Table 2: Charm cross-sections at HERA

Weizsäcker-Williams approximation. The results for charm production at HERA are summarised in Table 2. The contribution of the hadronic component has been included in the above results, using the photon structure functions of Ref. 10. The associated theoretical errors are very difficult to calculate; an estimate is given in Table 2. We have however verified that the hadronic component gives less than 30% contribution even at HERA energies.

Acknowledgement.

This work was completed at the Institute for Theoretical Physics of the University of Santa Barbara. The research was supported in part by the National Science Foundation under grant No. PHY82-17853, supplemented by funds from the National Aeronautics and Space Administration. We acknowledge useful discussions with the participants of the workshop. In addition we are grateful G. Altarelli for helpful comments.

References

[1] P. Nason, S. Dawson and R. K. Ellis, Fermilab-Pub-87/222-T, (December 1987). Nuclear Physics B (to be published).

[2] J. C. Collins, D. E. Soper and G. Sterman, *Nucl. Phys.* **B263** (1986) 37 .

[3] L. M. Jones and H. W. Wyld, *Phys. Rev.* **D17** (1978) 759 .

[4] For a review of charm photoproduction see S. D. Holmes, W. Lee and J. E. Wiss, *Ann. Rev. Nucl. Part. Sci.* **35** (1985) 397 .

[5] R. K. Ellis and Z. Kunszt, Fermilab-Pub-87/226-T, (December 1987). Nuclear Physics B (to be published).

[6] For the corresponding effect in hadroproduction see R. K. Ellis, Proceedings of the 21st Rencontre de Moriond, 'Strong Interactions and Gauge Theories', Editions Frontieres (1986), ed. J. Tran Thanh Van.

[7] W. A. Bardeen *et al.*, *Phys. Rev.* **D18** (1978) 3998 .

[8] G. Altarelli and G. Parisi, *Nucl. Phys.* **B126** (1977) 298

[9] G. Altarelli, R. K. Ellis and G. Martinelli, *Nucl. Phys.* **B242** (1984) 120 .

[10] M. Drees and K. Grassie, *Zeit. Phys.* **C28** (1985) 451

[11] M. Diemoz, F. Ferroni, E. Longo and G. Martinelli, CERN-TH-4751/87 (1987); J. V. Allaby *et al.*, *Phys. Lett.* **197B** (1987) 281 .

[12] G. Altarelli, M Diemoz, G. Martinelli and P. Nason, CERN-TH-4978/88 (1988).

[13] M.I. Adamovich *et al.*, (Photon Emulsion Collaboration), *Phys. Lett.* **187B** (1987) 437 .

[14] J. C. Anjos *et al.*, (E691) Fermilab preprint, (June, 1988).

[15] S. Narison, *Phys. Lett.* **197B** (1987) 405 .

Figure Captions

Fig. 1: Feynman diagrams for photon-gluon fusion.

Fig. 2: The photon gluon contributions to the parton cross-section plotted versus $1/\rho$. The functions $c^{(0)}, c^{(1)}$ and $\overline{c}^{(1)}$ are defined in eqs.(2.1, 2.4).

Fig. 3: The photon quark contributions proportional to the square of the heavy quark charge. The parton cross-section is plotted versus $1/\rho$. The functions $c^{(1)}$ and $\overline{c}^{(1)}$ are defined in eqs.(2.1, 2.4).

Fig. 4: The photon quark contributions proportional to the square of the light quark charge. The parton cross-section is plotted versus $1/\rho$. The functions $d^{(1)}$ and $\bar{d}^{(1)}$ are defined in eqs.(2.1, 2.4).

Fig. 5: Diagrams responsible for the constant behaviour of the parton cross-sections.

Fig. 6: The cross-section for the production of charm per unit of rapidity at $E_\gamma =$ 200 GeV.

Fig. 7: The cross-section for the production of charm per unit of rapidity at $\sqrt{S} =$ 314 GeV.

Fig. 8: The total cross-section for the photoproduction of a pair of charm quarks versus $\sqrt{S}$. The band of values represents an estimate of the theoretical uncertainty due to the variation of all parameters except the mass of the charm quark which is fixed at 1.2 GeV.

Fig. 9: The total cross-section for the photoproduction of a pair of charm quarks versus $\sqrt{S}$. The band of values represents an estimate of the theoretical uncertainty due to the variation of all parameters except the mass of the charm quark which is fixed at 1.5 GeV.

Fig. 10: The total cross-section for the photoproduction of a pair of charm quarks versus $\sqrt{S}$. The band of values represents an estimate of the theoretical uncertainty due to the variation of all parameters except the mass of the charm quark which is fixed at 1.8 GeV.

Fig. 11: The Feynman x_F dependence of the cross-section for the photoproduction of a charmed quark of mass $m = 1.5$ GeV for $E_\gamma = 150$ GeV. The contributions of both the lowest order and the total including radiative corrections are shown plotted.

Fig. 12: Comparison of the lowest order and next order predictions for the shape of the Feynman x_F dependence of the cross-section. Fragmentation has been included using the Peterson fragmentation function.

Fig. 13: The transverse momentum dependence of the cross-section for the photoproduction of a charmed quark of mass $m = 1.5$ GeV at $\sqrt{S} = 16.8$ GeV.

The contributions of both the lowest order and the total including radiative corrections are shown plotted.

Fig. 14: The dependence of the total cross-section for the photoproduction of a pair of bottom quarks on the parameter μ.

Fig. 15: The total cross-section for the photoproduction of a pair of bottom quarks versus E_γ. The band of values represents an estimate of the theoretical uncertainty due variation of all parameters including the mass of the bottom quark.

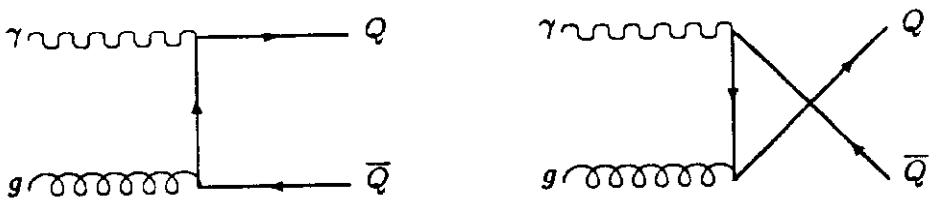
γ
Q
g
Q̄
γ
Q
g
Q̄

Fig. 1

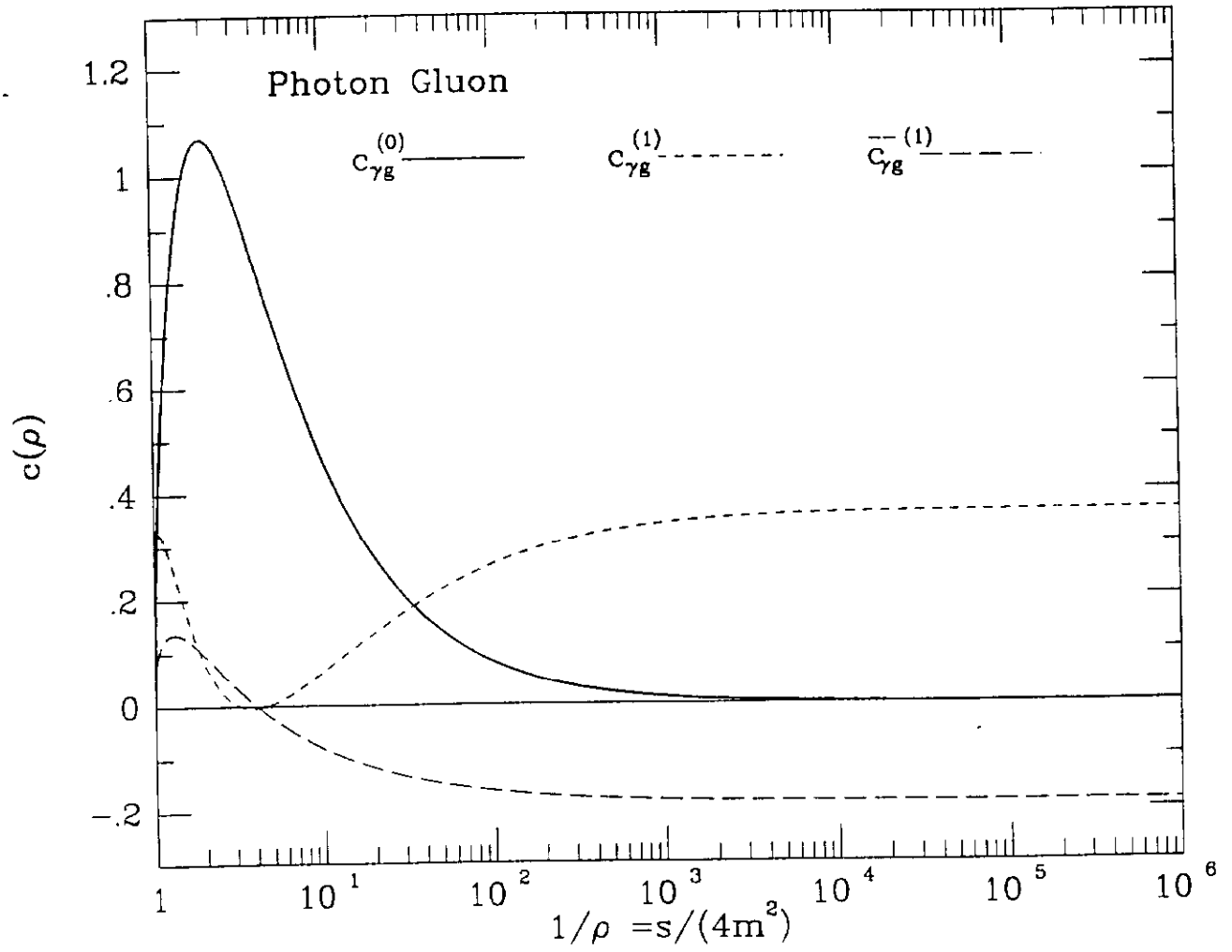
Photon Gluon
$c_{\gamma g}^{(0)}$
$c_{\gamma g}^{(1)}$
$\bar{c}_{\gamma g}^{(1)}$
c(ρ)
1.2
1
.8
.6
.4
.2
0
-.2
1
10 1
10 2
10 3
10 4
10 5
10 6
1/ρ =s/(4m²)

Fig. 2

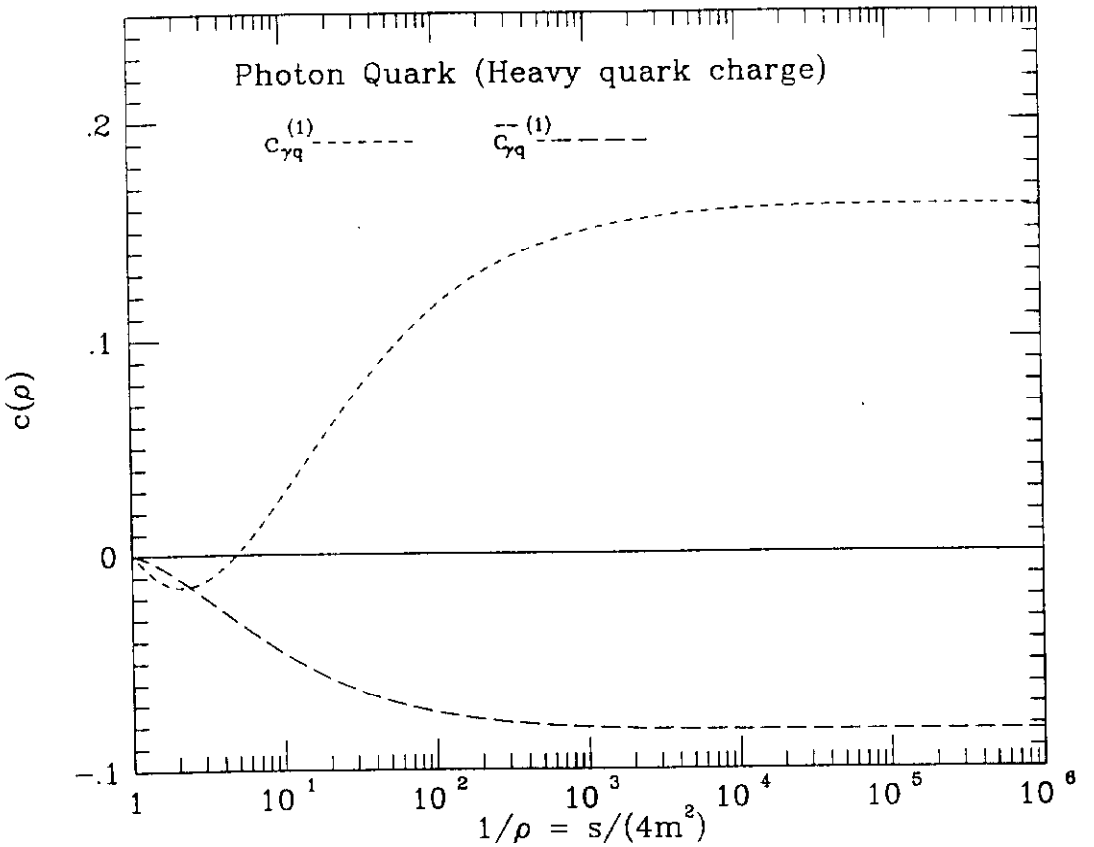
Photon Quark (Heavy quark charge)
$c_{\gamma q}^{(1)}$
$\bar{c}_{\gamma q}^{(1)}$
.2
.1
0
−.1
c(ρ)
1
10^1
10^2
10^3
10^4
10^5
10^6
$1/\rho = s/(4m^2)$

Fig. 3

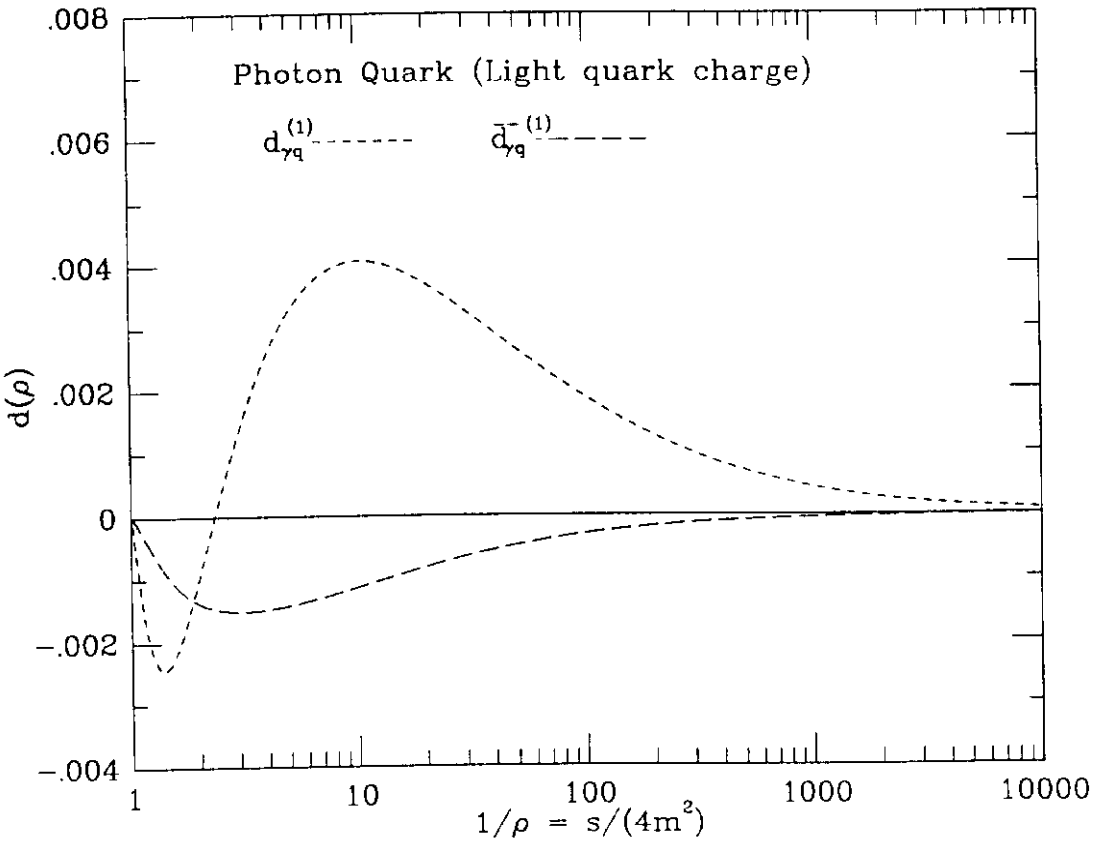
Photon Quark (Light quark charge)
$d_{\gamma q}^{(1)}$
$\bar{d}_{\gamma q}^{(1)}$
.008
.006
.004
.002
0
−.002
−.004
d(ρ)
1
10
100
1000
10000
$1/\rho = s/(4m^2)$

Fig. 4

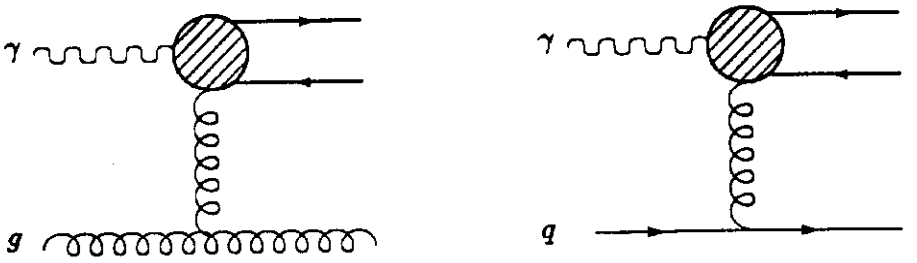

Fig. 5

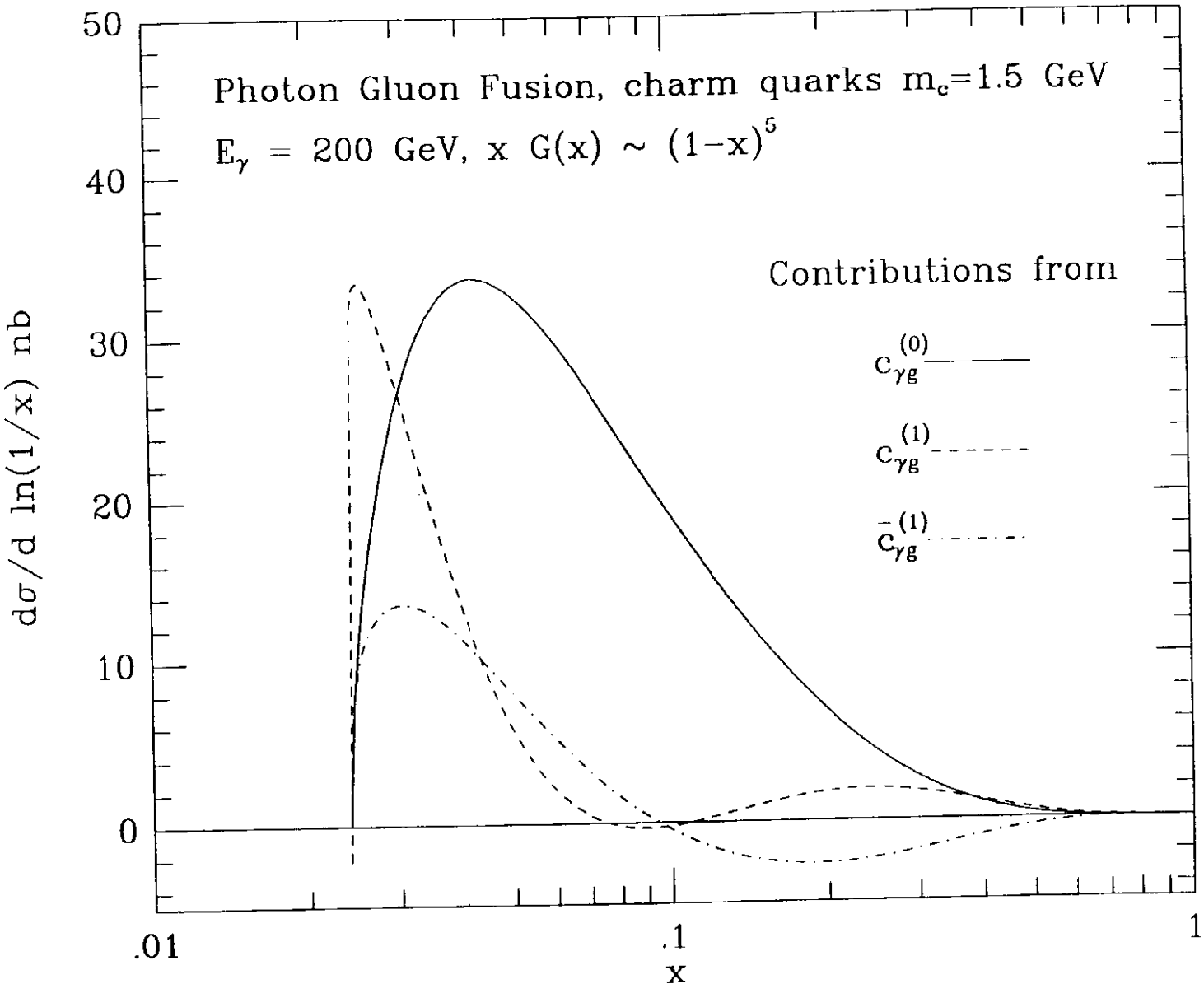
Photon Gluon Fusion, charm quarks m_c=1.5 GeV
E_γ = 200 GeV, x G(x) ~ $(1-x)^5$
Contributions from
$C_{\gamma g}^{(0)}$
$C_{\gamma g}^{(1)}$
$\bar{C}_{\gamma g}^{(1)}$
dσ/d ln(1/x) nb
50
40
30
20
10
0
.01
.1
1
x

Fig. 6

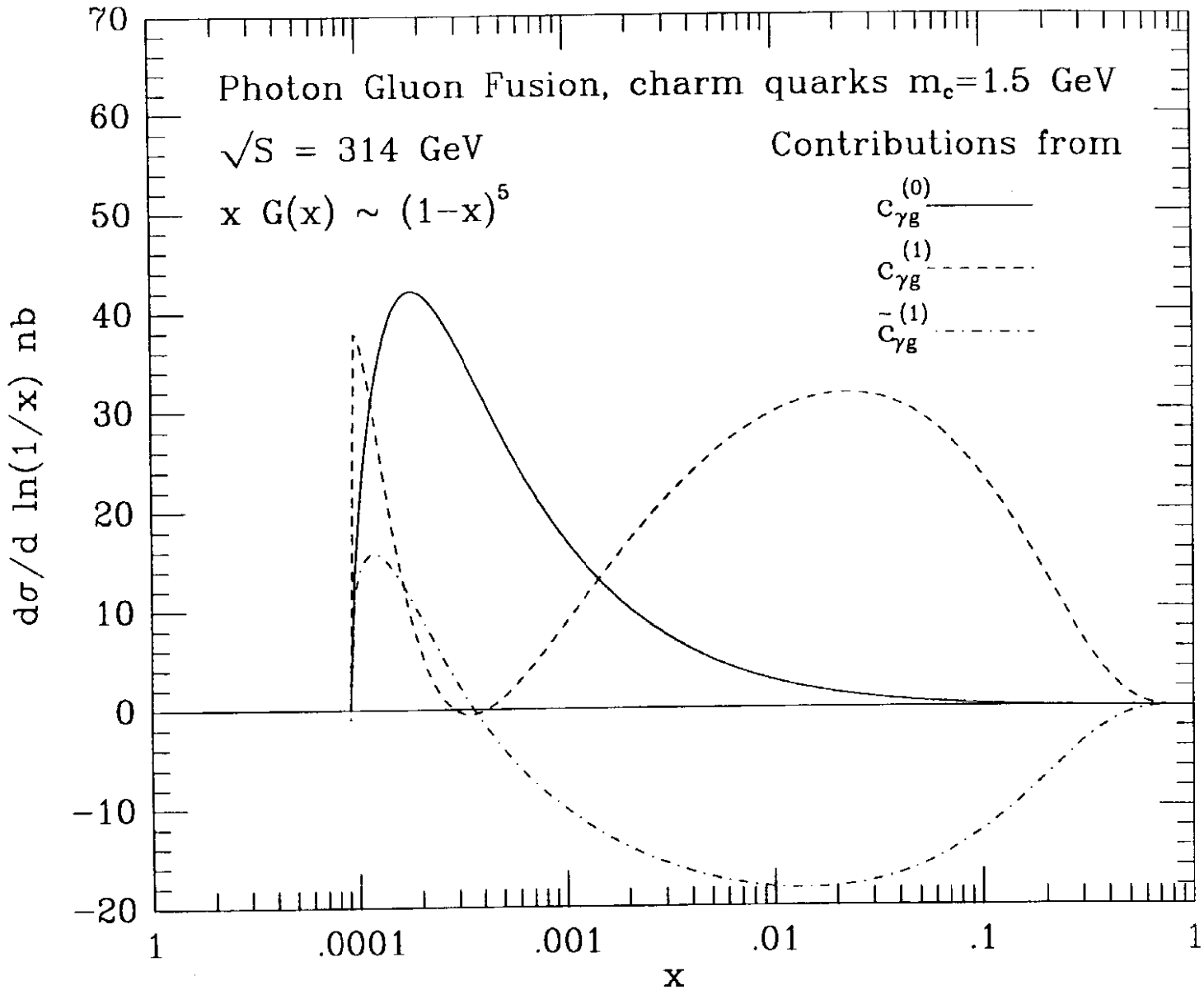
Photon Gluon Fusion, charm quarks m_c=1.5 GeV
$\sqrt{S}$ = 314 GeV
x G(x) ~ $(1-x)^5$
Contributions from
$c_{\gamma g}^{(0)}$
$c_{\gamma g}^{(1)}$
$\tilde{c}_{\gamma g}^{(1)}$
dσ/d ln(1/x) nb
x
70
60
50
40
30
20
10
0
−10
−20
1
.0001
.001
.01
.1
1

Fig. 7

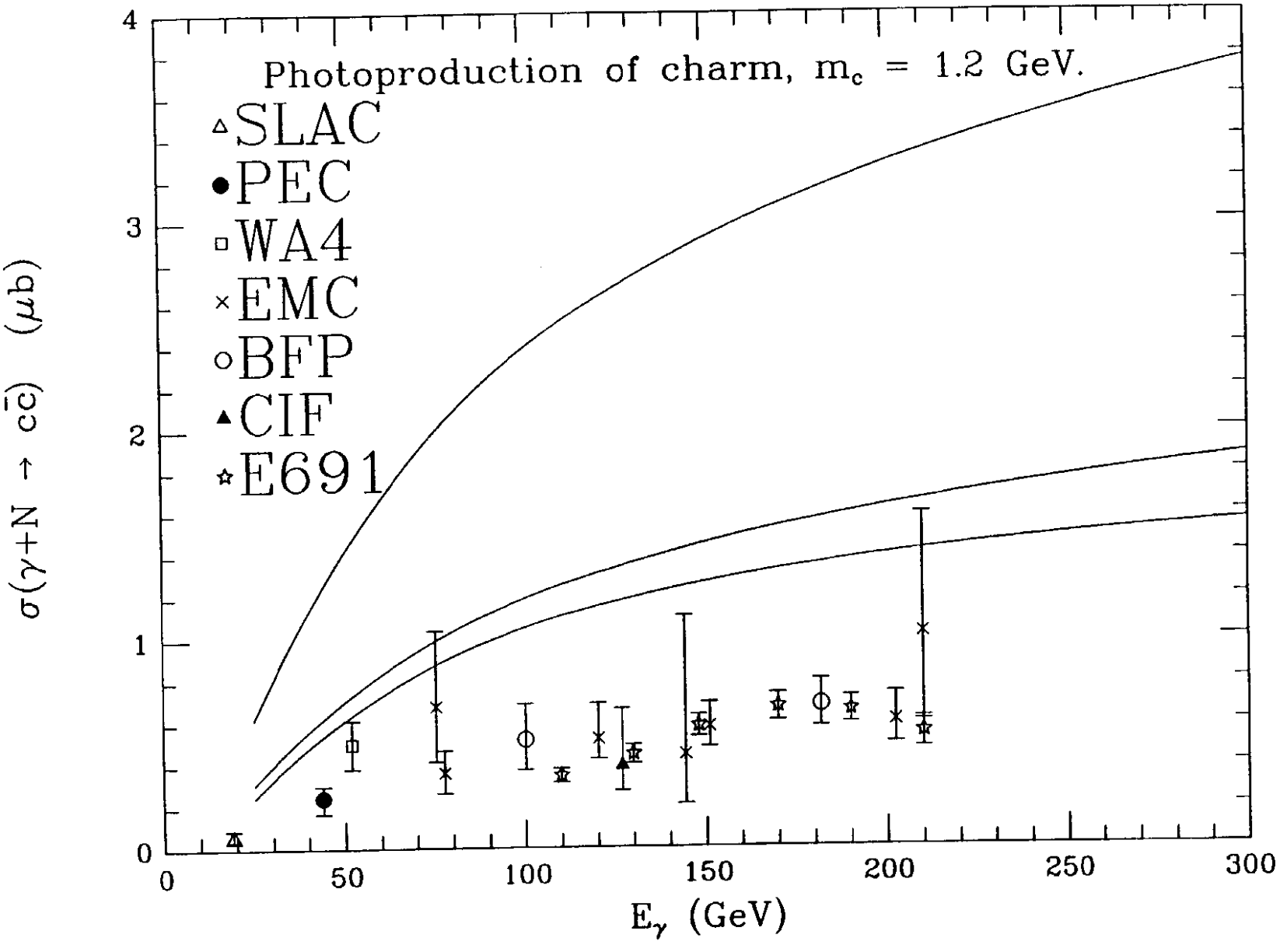
Photoproduction of charm, m_c = 1.2 GeV.
SLAC
PEC
WA4
EMC
BFP
CIF
E691
$\sigma(\gamma+N \rightarrow c\bar{c})$ (μb)
E_γ (GeV)
0
1
2
3
4
0
50
100
150
200
250
300

Fig. 8

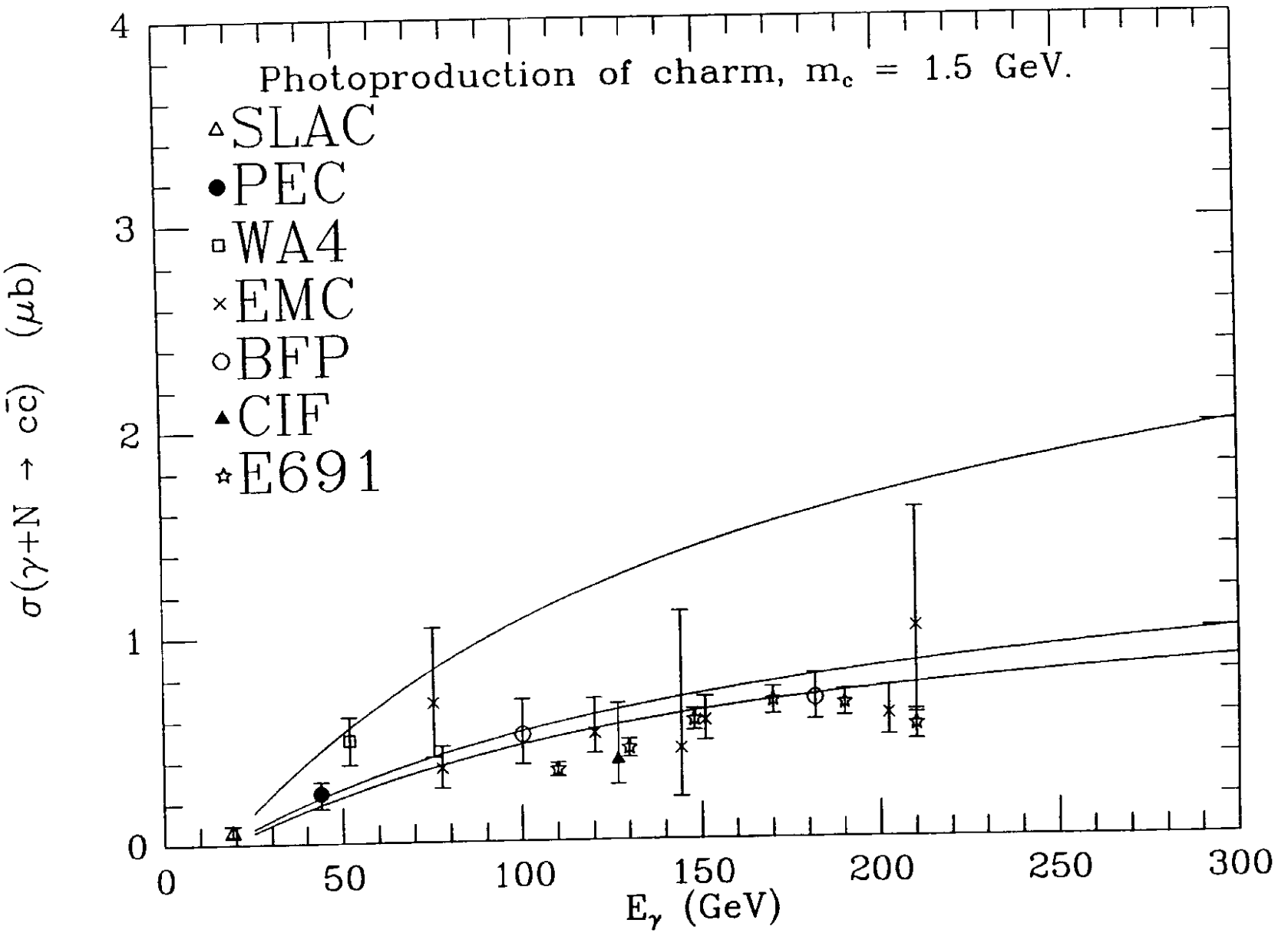
Photoproduction of charm, m_c = 1.5 GeV.
SLAC
PEC
WA4
EMC
BFP
CIF
E691
$\sigma(\gamma+N \rightarrow c\bar{c})$ (μb)
E_γ (GeV)
0
1
2
3
4
0
50
100
150
200
250
300

Fig. 9

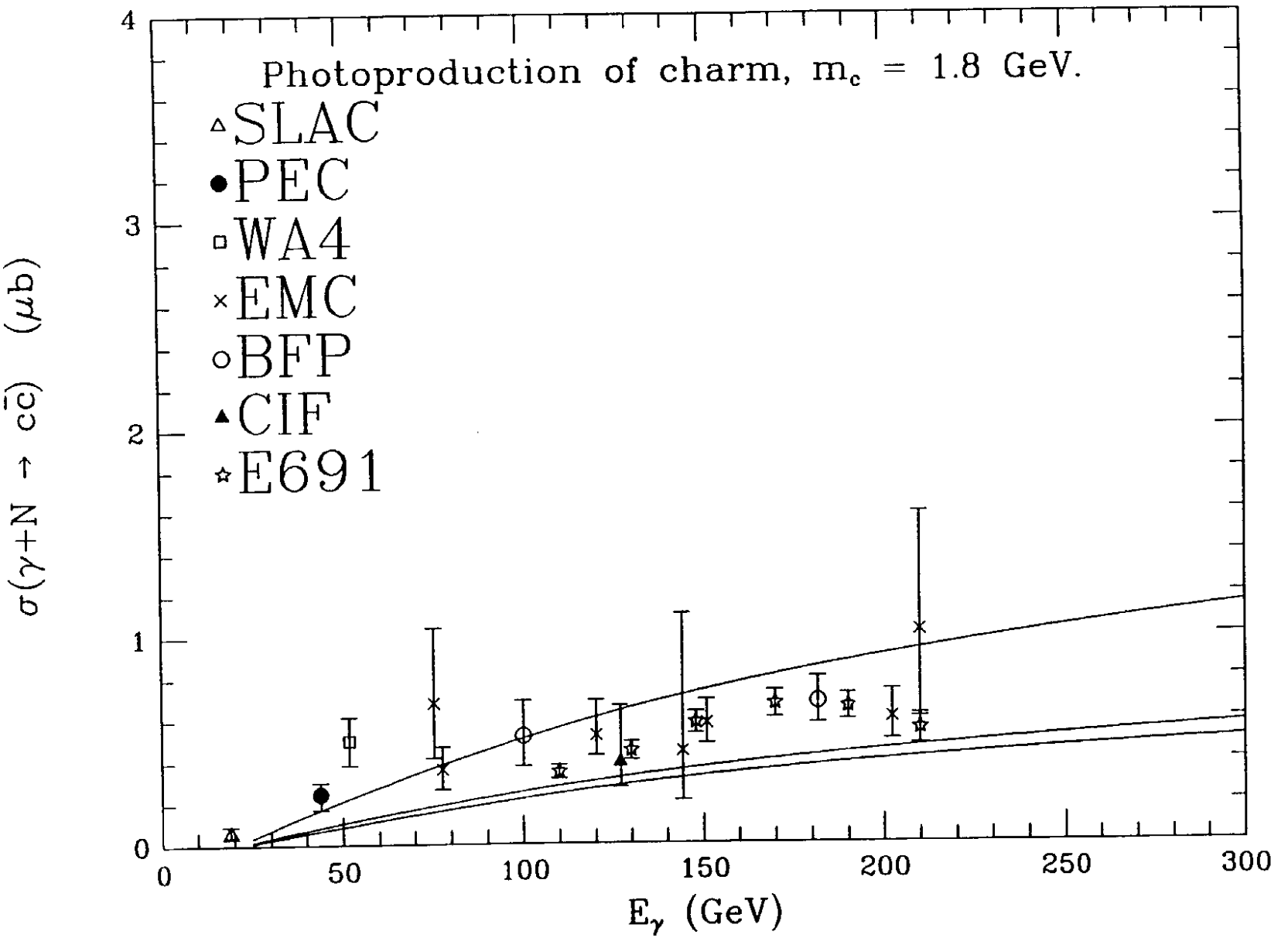
Photoproduction of charm, m_c = 1.8 GeV.
SLAC
PEC
WA4
EMC
BFP
CIF
E691
$\sigma(\gamma+N \rightarrow c\bar{c})$ (μb)
E_γ (GeV)
0
1
2
3
4
0
50
100
150
200
250
300

Fig. 10

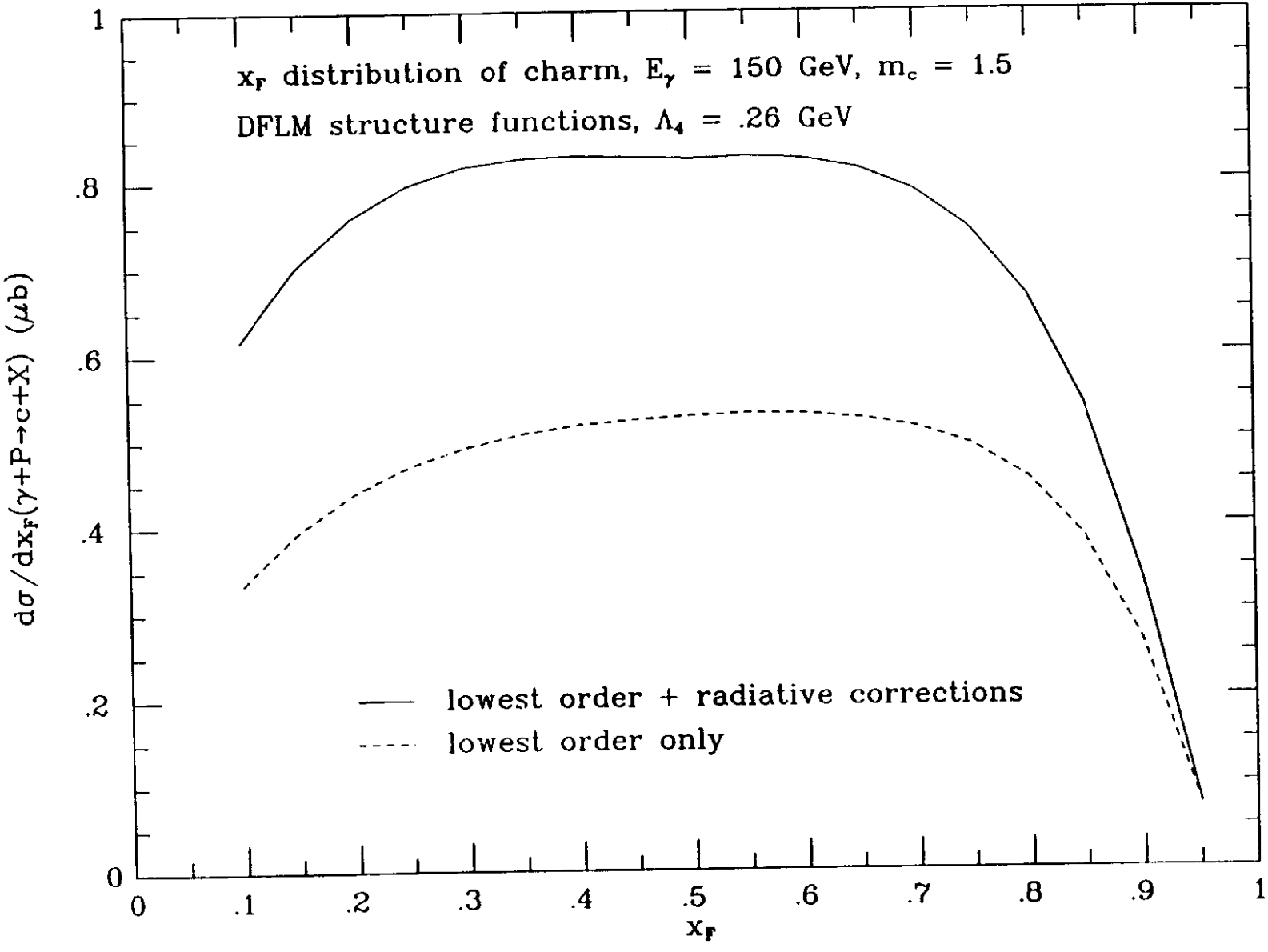
x_F distribution of charm, E_γ = 150 GeV, m_c = 1.5
DFLM structure functions, Λ_4 = .26 GeV
lowest order + radiative corrections
lowest order only
$d\sigma/dx_F(\gamma+P\rightarrow c+X)$ (μb)
x_F
0
.2
.4
.6
.8
1
.1
.3
.5
.7
.9

Fig. 11

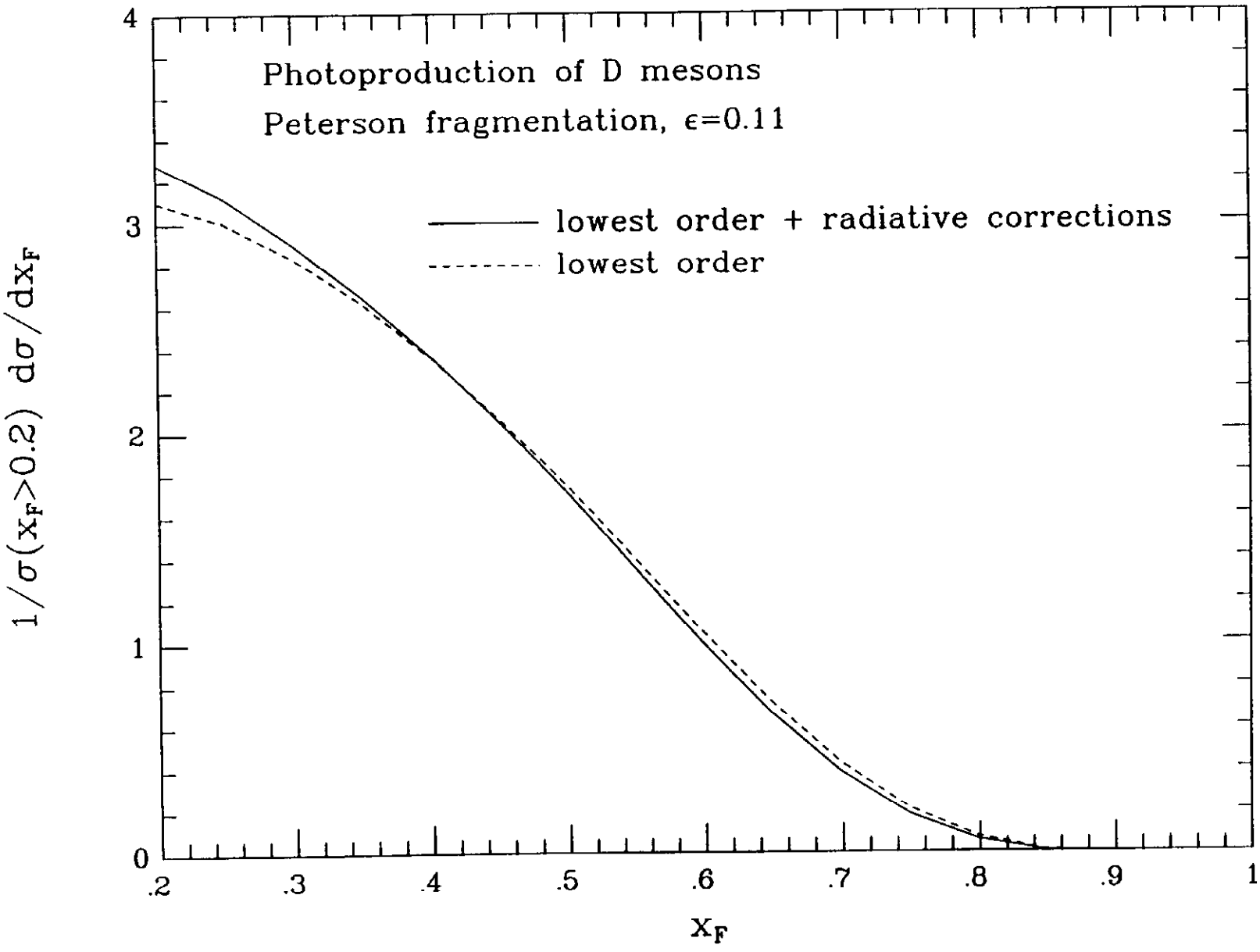
Photoproduction of D mesons
Peterson fragmentation, ε=0.11
lowest order + radiative corrections
lowest order
1/σ(x_F>0.2) dσ/dx_F
x_F
0
1
2
3
4
.2
.3
.4
.5
.6
.7
.8
.9
1

Fig. 12

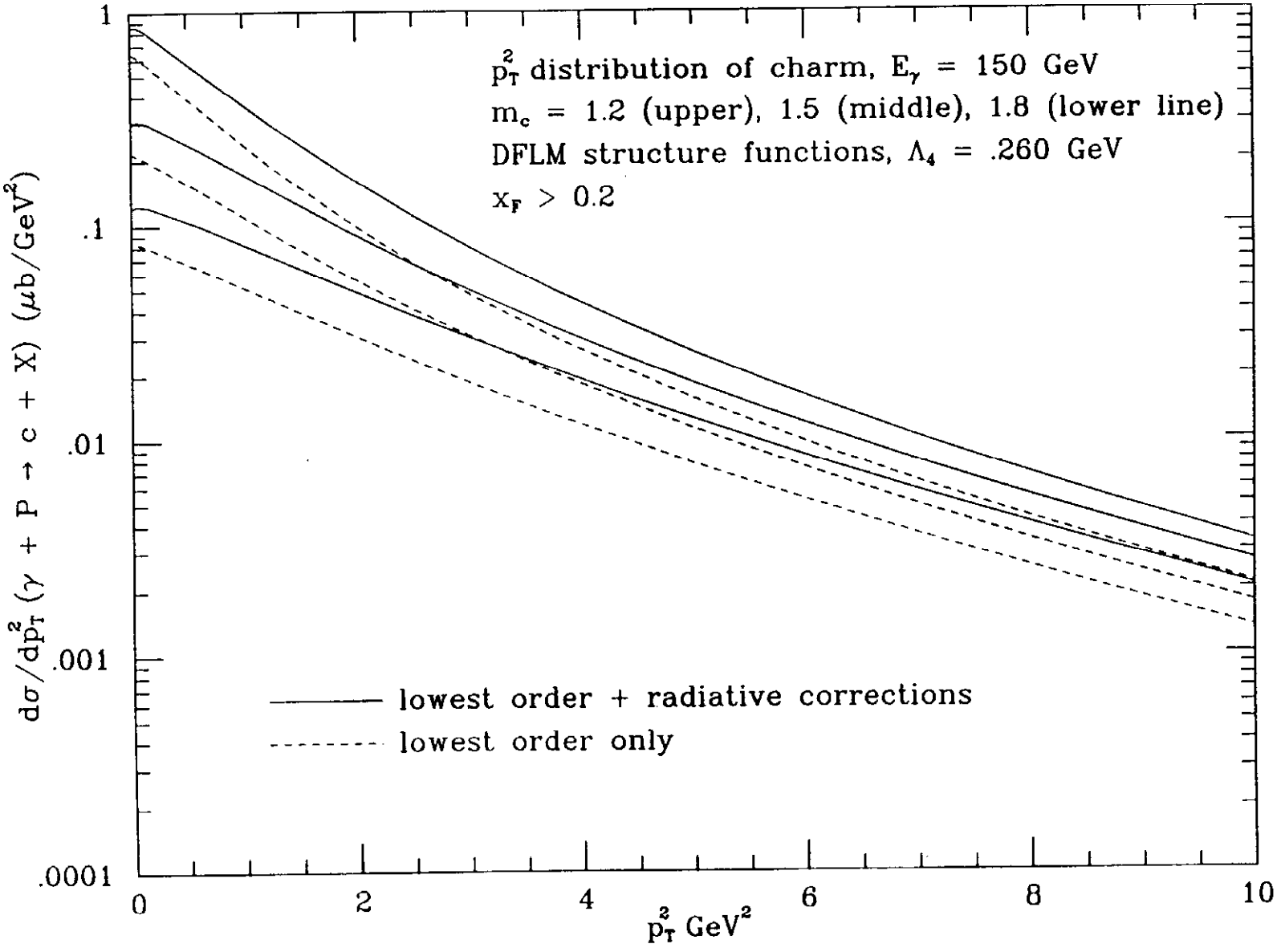
p_T^2 distribution of charm, E_γ = 150 GeV
m_c = 1.2 (upper), 1.5 (middle), 1.8 (lower line)
DFLM structure functions, Λ_4 = .260 GeV
$x_F > 0.2$
lowest order + radiative corrections
lowest order only
$d\sigma/dp_T^2\ (\gamma + P \rightarrow c + X)\ (\mu b/GeV^2)$
p_T^2 GeV^2
1
.1
.01
.001
.0001
0
2
4
6
8
10

Fig. 13

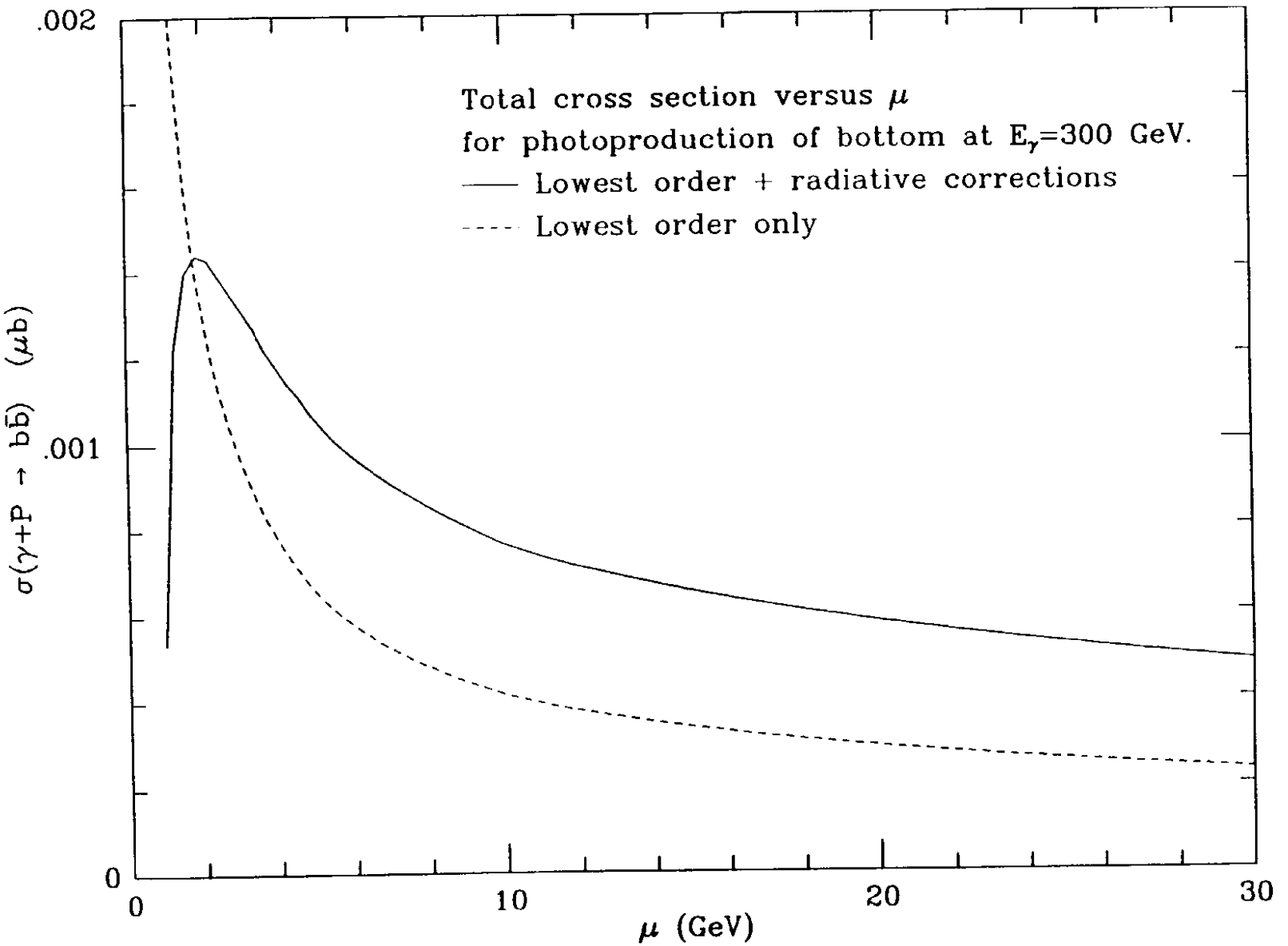
.002
.001
0
0
10
20
30
μ (GeV)
σ(γ+P → bb̄) (μb)
Total cross section versus μ
for photoproduction of bottom at E_γ=300 GeV.
—— Lowest order + radiative corrections
---- Lowest order only

Fig. 14

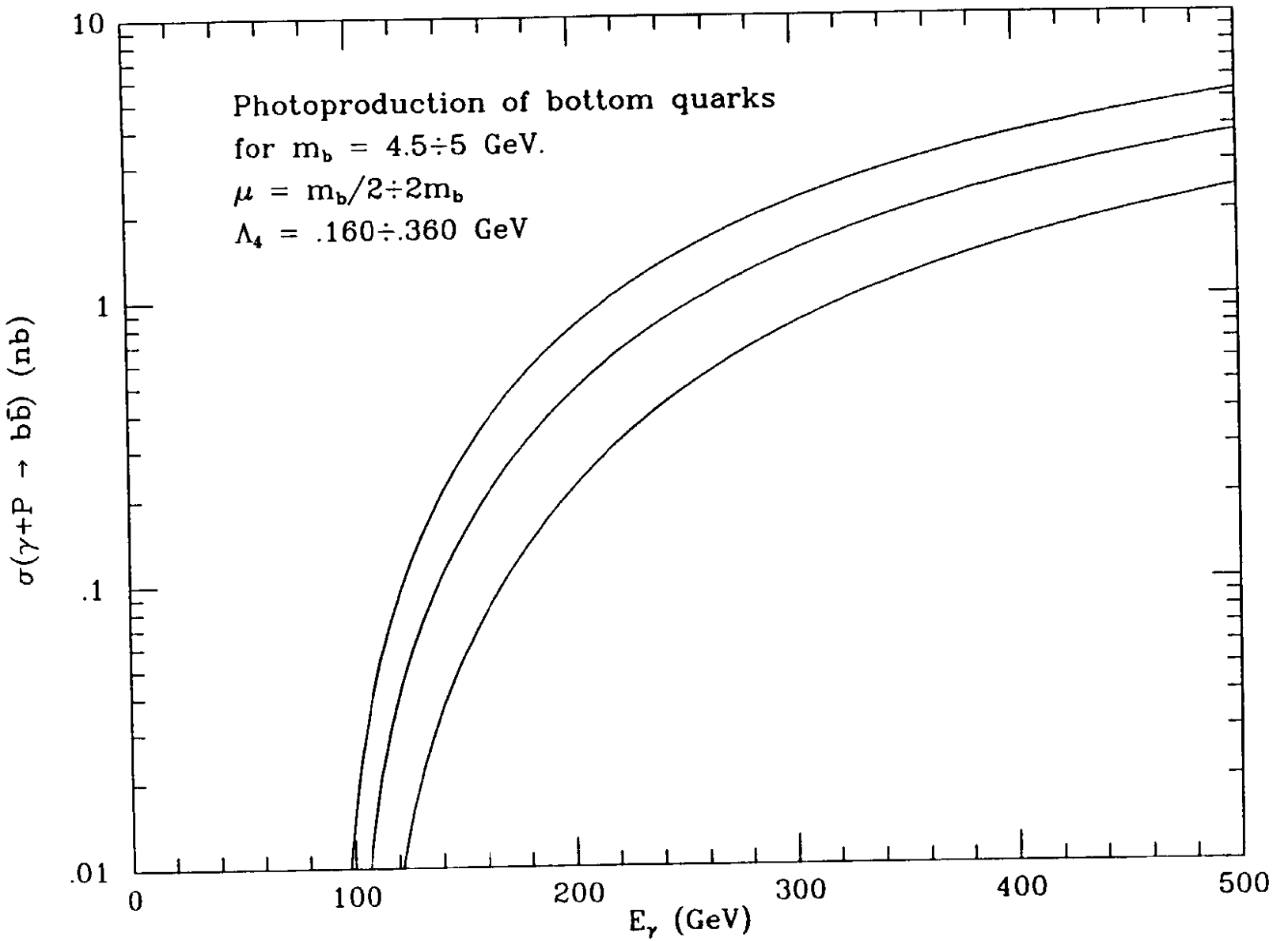
Photoproduction of bottom quarks
for m_b = 4.5÷5 GeV.
μ = $m_b/2 \div 2m_b$
Λ_4 = .160÷.360 GeV
10
1
.1
.01
0
100
200
300
400
500
E_γ (GeV)
$\sigma(\gamma+P \rightarrow b\bar{b})$ (nb)

Fig. 15